Supplementary Information
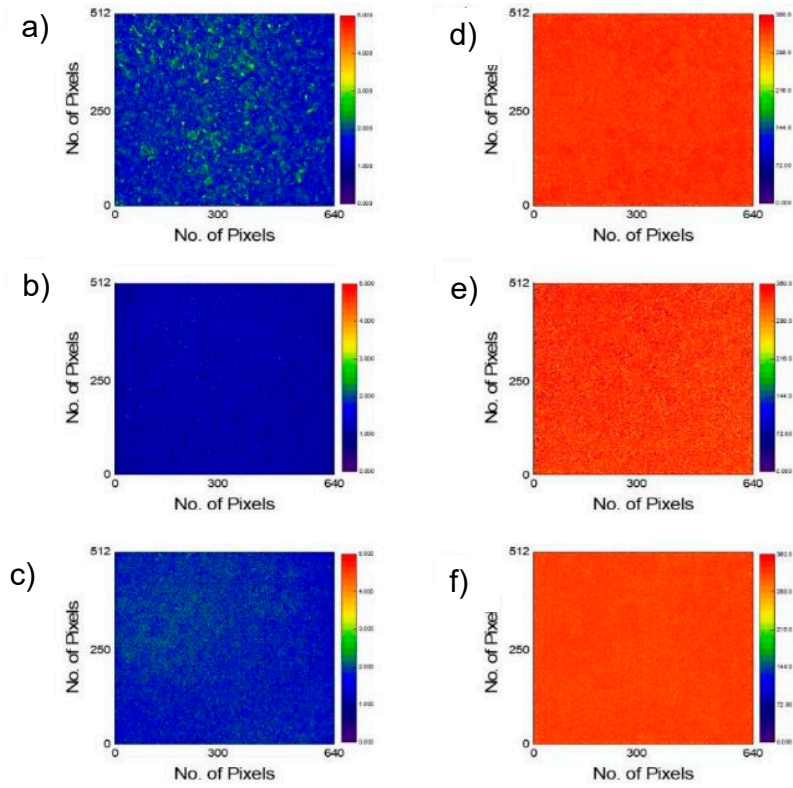

Figure S1. (a-c) Illuminated lock-in illumination amplitude images with scale bar indicating low amplitude to high amplitude of captured thermal emission; (d-f) Illumination phase images with scale bar indicating captured light being in-phase to out-of-phase of the light pulse; (a,d) 0% GG, (b,e) 0.18% GG, (c,f) 0.56% GG. All the images have a common scale of 4.6μm per pixel.
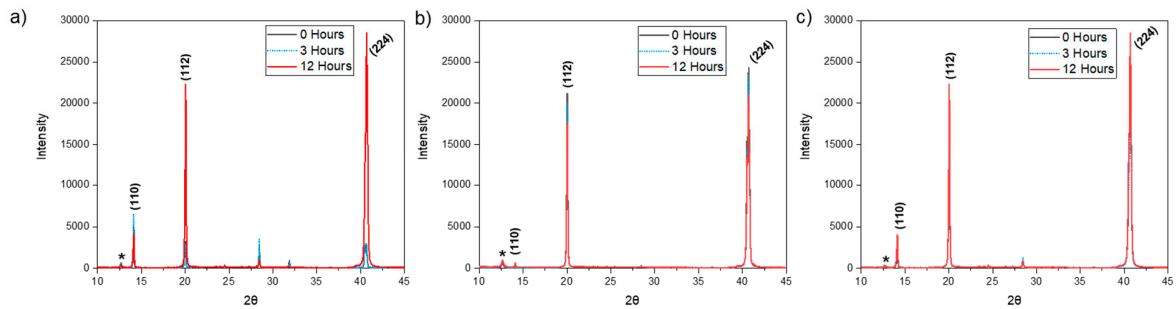

Figure S2. XRD spectrum of PVSK films before and after being exposed to 85°C for 12 hours. This is the same data that were previously plotted in Figure 5 (a-c) now on an extended 2θ axis for 0%, 0.18%, and 0.56% GG samples showing the change in orientational dominance induced by GG and heat aging which likely corresponds to stress relaxation in the film.
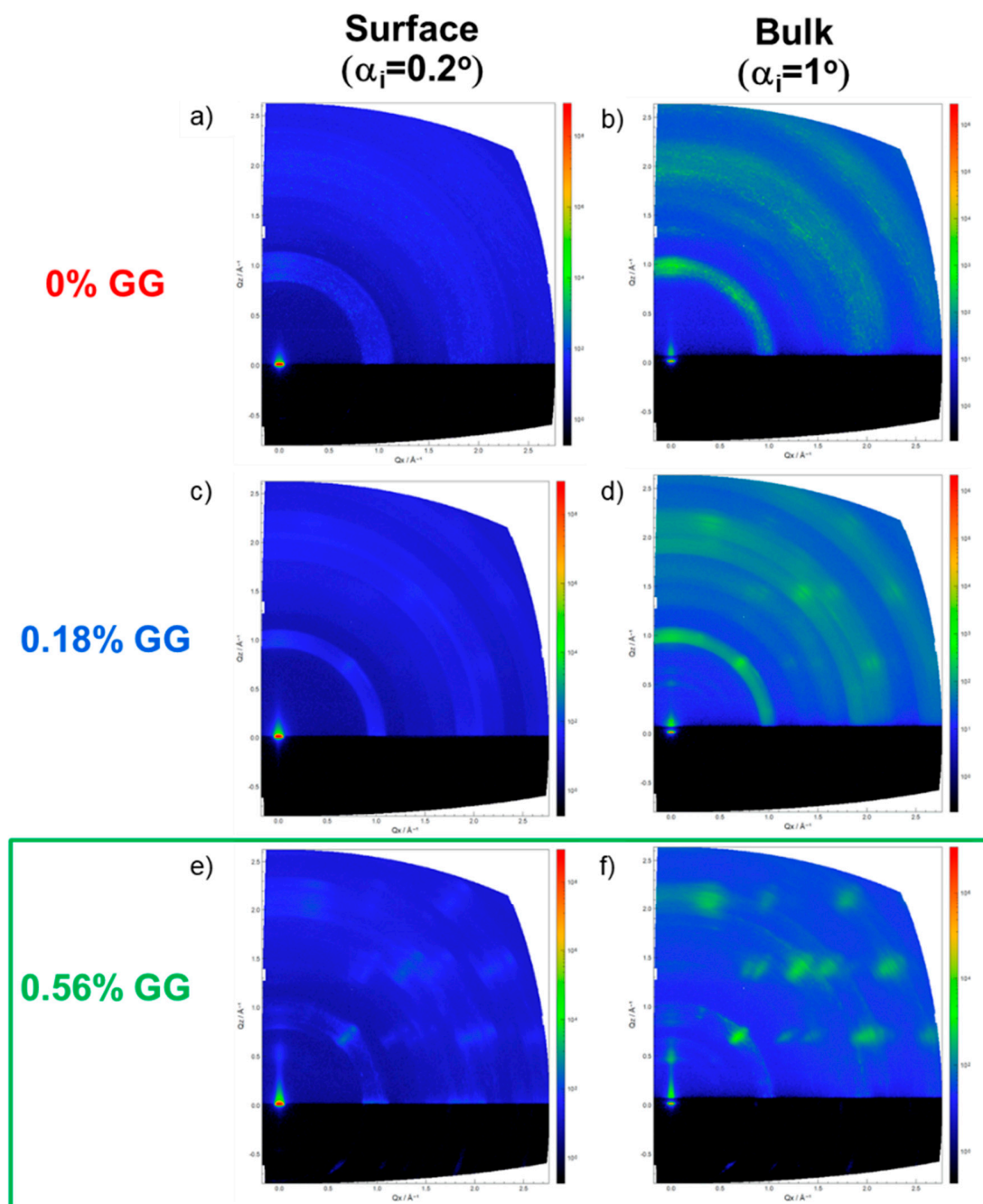
Figure S3. 2D (out of plane Qx-Qz where Qy is the beam direction) adjusted GIWAXS spectrums collected on as blade coated samples, (a-b) 0%GG, (c-d) 0.18%GG, and (e-f) 0.56%GG, at different penetration depths demonstrating stronger crystallographic texturing with increasing GG concentrations whereby the films transition from having randomly oriented 3D bulk crystal banding to a partially to highly oriented 3D bulk crystal structure in the 0.18% GG and optimized 0.56% GG films. Band distortion and outward smearing is thought to be due to the instrumentation and stage set-up rather than a crystallographic feature.
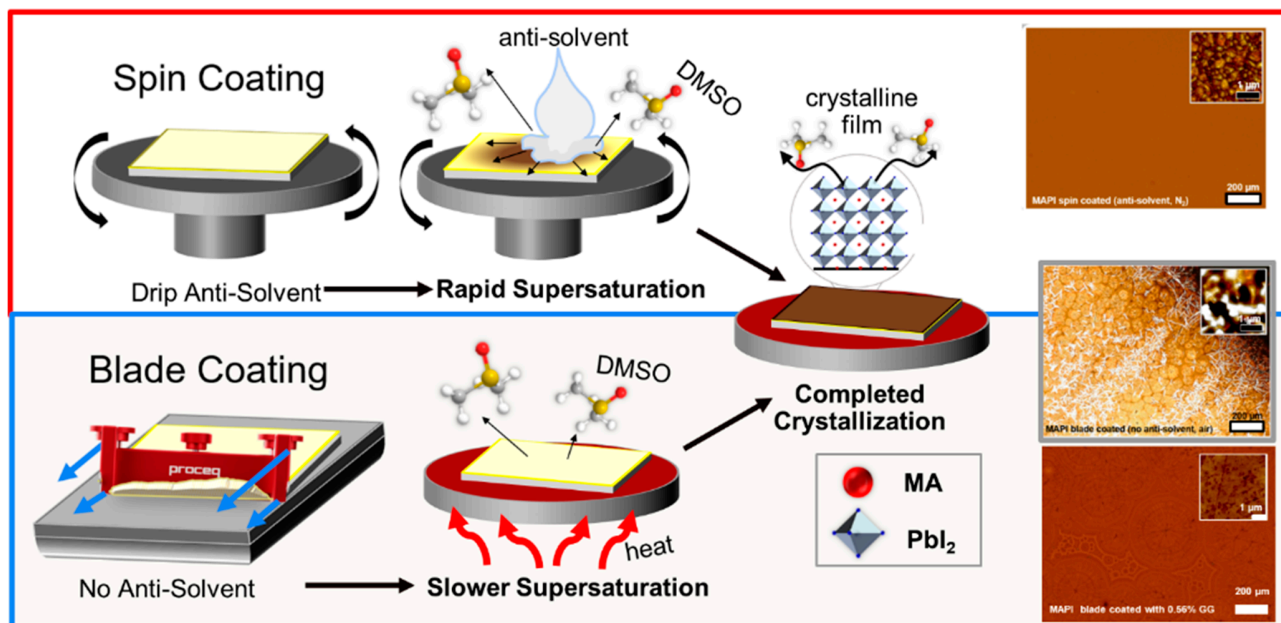
Figure S4. Schematic of the preparation process showing an example of use of an antisolvent quench while spin coating with corresponding optical and AFM height image which demonstrate that the rapid targeted solvent evaporation drives a high rate and degree of supersaturation causing dense burst nucleation and small regularly sized grains while blade coating without an antisolvent can cause uneven films unless properly modified such as with 0.56%GG which features a distinct compact morphology with larger radial domains.
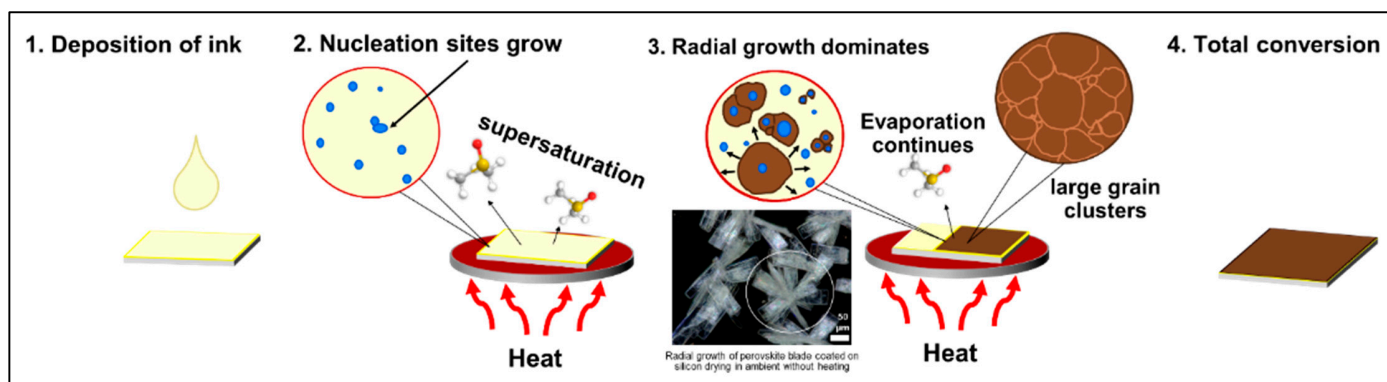

Figure S5. Summary of the crystallization process from initial deposition to the nucleation dominated regime, growth regime (with an associated optical image taken in-situ during the non-heat assisted crystallization of a blade coated perovskite film on a silicon wafer), and finally complete film conversion.
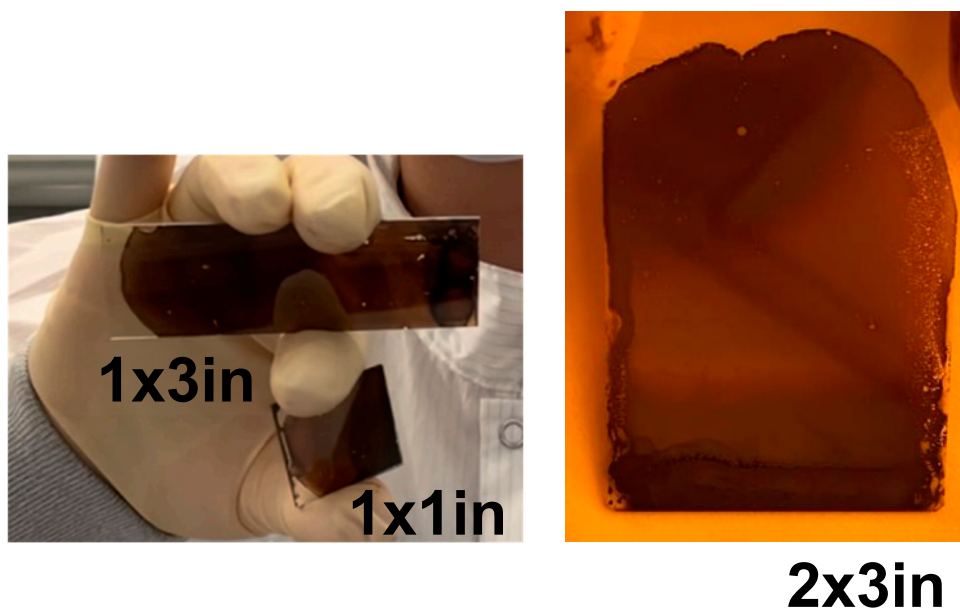
Figure S6. Images depicting the ability of scale up using GG with ambient doctor blade coating.

Abbreviation	Expanded Term
PVSK, MAPI	perovskite, methylammonium lead iodide ($CH_3NH_3PbI_3$)
ITO	Indium Tin Oxide
GG	gellan gum
C, Cs, C*, C*min, C*max	Concentration, saturation concentration which marks the classical critical concentration for which growth can occur, critical supersaturation concentration marks the classical critical concentration from which the nucleation regime dominates, C^*_{min} and C^*_{max} denote the minimum and maximum concentrations from which stable nucleates are likely to form with a concentration having once exceeded and then dropping below C*min showing a transition to the growth dominated regime
XRD, GIWAXS, PL, ILIT	X-ray diffraction, grazing incidence wide angle X-ray scattering, photoluminescence spectroscopy, illuminated lock-in thermography

Table S1: An abbreviation and nomenclature list associated with commonly used terms in the body of the main text

Sample	Series Resistance (R_s) (Ω)	Shunt Resistance (R_{sh}) (Ω)
0% GG	181.21 ± 33.74	165 ± 42.47
0.18% GG	440 ± 83.18	$2.69 * 10^3 \pm 1.081 * 10^3$
0.56% GG	54.8 ± 35.76	$2.43 * 10^5 \pm 8.2 * 10^4$

Table S2: Series and Shunt resistances of the samples with 0% GG, 0.18% GG, and 0.56% GG respectively, with the sample having 0.56% GG showing the desired properties of the lowest amount of series resistance and the highest amount of shunt resistance.